3000 *Chem. Mater.* **2010,** *22,* 3000–3008
DOI:10.1021/cm100514r

CHEMISTRY OF MATERIALS
Article

Synthesis and Electropolymerization of Hexadecyl Functionalized Bithiophene and Thieno[3,2-*b*]thiophene End-Capped with EDOT and EDTT Units

Greg J. McEntee,[†] Peter J. Skabara,*[,†] Filipe Vilela,[†] Steven Tierney,[‡] Ifor D. W. Samuel,[§] Salvatore Gambino,[§] Simon J. Coles,[⊥] Michael B. Hursthouse,[⊥] Ross W. Harrington,[#] and William Clegg[#]

[†]*WestCHEM, Department of Pure and Applied Chemistry, University of Strathclyde, Glasgow G1 1XL, United Kingdom,* [‡]*Merck Chemicals, Southampton SO16 7QD, United Kingdom,* [§]*Organic Semiconductor Centre, SUPA, School of Physics and Astronomy, University of St. Andrews, North Haugh, St. Andrews, Fife, KY16 9SS, United Kingdom,* [⊥]*School of Chemistry, University of Southampton, Southampton SO17 1BJ, United Kingdom, and* [#]*School of Chemistry, Newcastle University, Newcastle upon Tyne NE1 7RU, United Kingdom*

Received February 18, 2010. Revised Manuscript Received March 19, 2010

The synthesis of three novel thiophene-based conjugated molecules (**1**−**3**) is presented. We report the electronic and redox properties of these compounds along with the corresponding electrochemically prepared polymers. The structures of compounds **1** and **2** have been confirmed by single-crystal X-ray diffraction studies. Noncovalent S···O interactions in **1** act to hold the molecule in a planar conformation and this is in stark contrast to the twisted nature of the 3,4-ethylenedithiothiophene (EDTT) analogue. The degree of planarity within the molecules dictates the effective conjugation length within the materials and also the packing of the molecules in the solid state. CGL-TOF studies give hole mobilities up to 4×10^{-5} cm^2 V^{-1} s^{-1} for compound **1** and 1.5×10^{-5} cm^2 V^{-1} s^{-1} for **2**.

Introduction

Since the discovery by Shirakawa and co-workers that polyacetylene could be electrically conducting in its doped state,[1] conjugated polymers and small molecules have been widely investigated for use as semiconductors in organic electronic devices.[2−5] They have proved useful in applications including sensors,[6−9] electrochromics,[10−13] organic light-emitting diodes,[14−17] photovoltaics,[18−21] and field effect transistors.[3,4,22] These organic materials are attractive alternatives to their inorganic counterparts such as amorphous silicon because of cost-effective processability of the materials through solution deposition methods such as inkjet printing, spin coating and screen printing.[3,23,24] Such materials will be useful in producing large-area electronics onto mechanically flexible substrates.[25,26] Some thiophene-based polymers have shown charge carrier mobilities ranging from 0.1 to 1 cm^2 V^{-1} s^{-1},[27] values that are comparable to the benchmark standard of amorphous silicon.[28] Within this group of

*Corresponding author. E-mail: peter.skabara@strath.ac.uk.

(1) Chiang, C. K.; Fincher, C. R.; Park, Y. W.; Heeger, A. J.; Shirakawa, H.; Louis, E. J.; Gau, S. C.; Macdiarmid, A. G. *Phys. Rev. Lett.* **1977**, *39*(17), 1098.
(2) Dimitrakopoulos, C. D.; Malenfant, P. R. L. *Adv. Mater.* **2002**, *14* (2), 99.
(3) Allard, S.; Forster, M.; Souharce, B.; Thiem, H.; Scherf, U. *Angew. Chem., Int. Ed.* **2008**, *47*(22), 4070.
(4) Mas-Torrent, M.; Rovira, C. *Chem. Soc. Rev.* **2008**, *37*(4), 827.
(5) Newman, C. R.; Frisbie, C. D.; daSilvaFilho, D. A.; Bredas, J. L.; Ewbank, P. C.; Mann, K. R. *Chem. Mater.* **2004**, *16*(23), 4436.
(6) Goldenberg, L. M.; Skabara, P. J.; Roberts, D. M.; Berridge, R.; Orti, E.; Viruela, P. M.; Pou-Amerigo, R. *J. Mater. Chem.* **2000**, *10* (11), 2458.
(7) Ho, H.-A.; Leclerc, M. *J. Am. Chem. Soc.* **2004**, *126*(5), 1384.
(8) Locklin, J.; Bao, Z. N. *Anal. Bioanal. Chem.* **2006**, *384*(2), 336.
(9) Hui, J.; Prasad, T.; John, R. R.; Kirk, S. S. *Angew. Chem., Int. Ed.* **2009**, *48*(24), 4300.
(10) Mortimer, R. J.; Dyer, A. L.; Reynolds, J. R. *Displays* **2006**, *27*(1), 2.
(11) Sonmez, G.; Sonmez, H. B.; Shen, C. K. F.; Jost, R. W.; Rubin, Y.; Wudl, F. *Macromolecules* **2005**, *38*(3), 669.
(12) Cirpan, A.; Argun, A. A.; Grenier, C. R. G.; Reeves, B. D.; Reynolds, J. R. *J. Mater. Chem.* **2003**, *13*(10), 2422.
(13) Roncali, J. *Macromol. Rapid Commun.* **2007**, *28*(17), 1761.
(14) Burroughes, J. H.; Bradley, D. D. C.; Brown, A. R.; Marks, R. N.; Mackay, K.; Friend, R. H.; Burns, P. L.; Holmes, A. B. *Nature* **1990**, *347*(6293), 539.
(15) Arno, K.; Andrew, C. G.; Andrew, B. H. *Angew. Chem., Int. Ed.* **1998**, *37*(4), 402.
(16) Forrest, S. R. *Nature* **2004**, *428*(6986), 911.
(17) Dini, D. *Chem. Mater.* **2005**, *17*(8), 1933.
(18) Segura, J. L.; Martin, N.; Guldi, D. M. *Chem. Soc. Rev.* **2005**, *34*(1), 31.
(19) Gunes, S.; Neugebauer, H.; Sariciftci, N. S. *Chem. Rev.* **2007**, *107* (4), 1324.
(20) Lloyd, M. T.; Anthony, J. E.; Malliaras, G. G. *Mater. Today* **2007**, *10*(11), 34.
(21) Kippelen, B.; Bredas, J.-L. *Energy Environ. Sci.* **2009**, *2*(3), 251.
(22) Facchetti, A. *Mater. Today* **2007**, *10*(3), 28.
(23) Chabinyc, M. L.; Salleo, A. *Chem. Mater.* **2004**, *16*(23), 4509.
(24) Menard, E.; Meitl, M. A.; Sun, Y.; Park, J. U.; Shir, D. J. L.; Nam, Y. S.; Jeon, S.; Rogers, J. A. *Chem. Rev.* **2007**, *107*(4), 1117.
(25) Sirringhaus, H. *Adv. Mater.* **2005**, *17*(20), 2411.
(26) Shuhong, L.; Wechung Maria, W.; Alejandro, L. B.; Stefan, C. B. M.; Zhenan, B. *Adv. Mater.* **2009**, *21*(12), 1217.
(27) Brocorens, P.; Vooren, A. V.; Chabinyc, M. L.; Toney, M., F.; Shkunov, M.; Heeney, M.; McCulloch, I.; Cornil, J.; Lazzaroni, R. *Adv. Mater.* **2009**, *21*(10−11), 1193.
(28) McCulloch, I.; Heeney, M.; Bailey, C.; Genevicius, K.; Macdonald, I.; Shkunov, M.; Sparrowe, D.; Tierney, S.; Wagner, R.; Zhang, W. M.; Chabinyc, M. L.; Kline, R. J.; McGehee, M. D.; Toney, M. F. *Nat. Mater.* **2006**, *5*(4), 328.

Published on Web 04/02/2010

Chart 1

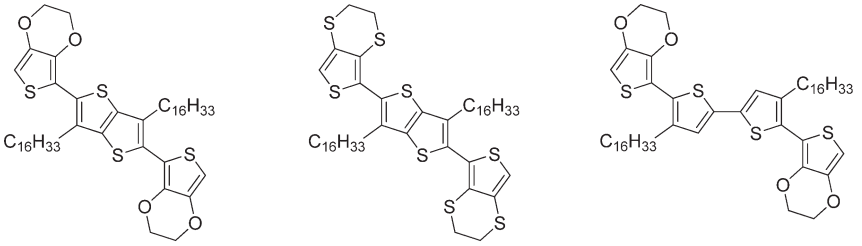

materials, thienothiophene-containing polymers have demonstrated some of the highest charge-carrier mobilities.[29] The specific values are dependent on a number of factors, including the physical architecture of the device,[30] choice of source-drain electrodes, and choice of dielectric material.[31] Charge carrier mobilities are also closely linked to the supramolecular arrangement of a material in the solid state.[27] It is important to align the semiconductor in such a way as to maximize charge transport between the source and drain electrodes through long-range $\pi-\pi$ interactions.[32]

Recently, Frère et al. reported oligomers containing an EDOT-thienothiophene motif. It was postulated that the oligomers presented a planar conformation due to the combination of rigid components and noncovalent effects.[33] In this paper, the synthesis and characterization of three novel thiophene-based molecules are reported. Compounds **1**−**3** have been designed such that noncovalent intramolecular interactions and their influence on the supramolecular structure of the molecules could be determined. Polymers of **1**−**3** were prepared electrochemically and their properties have been examined using cyclic voltammetry, UV−vis spectroscopy, and spectroelectrochemistry. Compound **1** was designed to include a fused alkyl-substituted thienothiophene core unit flanked by two EDOT units. For PEDOT and EDOT-containing copolymers, noncovalent S···O interactions act to enforce planarity, thus increasing the extent of π orbital overlap and, in turn, decreasing the HOMO−LUMO gap relative to a conformationally free equivalent. In **2**, the EDOT units have been replaced with 3,4-ethylenedithiothiophene (EDTT), in which the 3,4 bridge positions are occupied by sulfur atoms instead of oxygen. It has been shown that S···S interactions are more sterically demanding than S···O contacts;[34,35] thus, it was predicted that the molecule of compound **2** would be less planar than **1**. Such a configuration would affect the extent of π conjugation through the system and, as a result, the HOMO−LUMO energies. Compound **3** has retained the EDOT units, but the central thienothiophene has been replaced by a bithiophene unit. Compound **3** is expected to exhibit the same S···O interactions between EDOT and thiophene units but the molecule may not display the same planarity that is achieved by the presence of the fused thienothiophene in **1**. Indeed, crystallographic and electrochemical analysis confirm that **1** is held planar and that **2** is highly twisted, thus affecting the HOMO−LUMO energy gaps of the system. Electrochemical analysis of **3** indicates that a longer effective conjugation through the monomer unit results in a lower HOMO−LUMO energy gap than either compound **1** or **2** (see Chart 1).

Results and Discussion

Synthesis. The synthetic route to compounds **1**−**3** is summarized in Scheme 1. 2,5-Dibromo-3,6-dihexadecylthieno[3,2-b]thiophene **4** was prepared following a previously reported synthetic route.[29,36] Microwave-assisted Stille coupling of **4** with 2-trimethylstannyl derivatives of EDOT and EDTT gave compounds **1** and **2** in yields of 72 and 61%, respectively. Dibromo-4,4′-dihexadecyl-2,2′-bithiophene **5**[37] was also coupled with 2-trimethylstannyl EDOT to give compound **3** in 63% yield. Thermogravimetric analyses of compounds **1**−**3** showed that the materials begin to decompose in the range 350−370 °C, with the EDOT derivative being the least stable and the EDTT analogue the most resistant to higher temperatures. Differential scanning calorimetry revealed sharp melting points, but no phase transitions for any of the series.

Crystallography. Figure 1 shows the centrosymmetric molecule of compound **1**, in which the hydrogen atoms have been omitted for clarity. The EDOT-thienothiophene core unit is essentially planar (maximum deviation from planarity, measured by dihedral angles between planar segments, is 4.95°), and the two hexadecyl chains are angled at 40° relative to the plane of the thienothiophene core. The conjugated chain is held in a planar

(29) McCulloch, I.; Heeney, M.; Chabinyc, M. L.; DeLongchamp, D.; Kline, R. J.; Cölle, M.; Duffy, W.; Fischer, P.; Gundlach, D. J.; Hamadani, B. H.; Hamilton, R.; Richter, L.; Salleo, A.; Shkunov, M.; Sparrowe, D.; Tierney, S.; Zhang, W. *Adv. Mater.* **2009**, *21* (10−11), 1091.
(30) Di, C.-a.; Yu, G.; Liu, Y.; Zhu, D. *J. Phys. Chem. B* **2007**, *111*(51), 14083.
(31) Noh, Y.-Y.; Sirringhaus, H. *Org. Electron.* **2009**, *10*(1), 174.
(32) Pang, H.; Vilela, F.; Skabara, P. J.; McDouall, J. J. W.; Crouch, D. J.; Anthopoulos, T. D.; Bradley, D. D. C.; De Leeuw, D. M.; Horton, P. N.; Hursthouse, M. B. *Adv. Mater.* **2007**, *19*, 4438.
(33) Turbiez, M.; Hergue, N.; Leriche, P.; Frere, P. *Tetrahedron Lett.* **2009**, *50*(51), 7148.
(34) Turbiez, M.; Frere, P.; Allain, M.; Gallego-Planas, N.; Roncali, J. *Macromolecules* **2005**, *38*(16), 6806.
(35) Spencer, H. J.; Skabara, P. J.; Giles, M.; McCulloch, I.; Coles, S. J.; Hursthouse, M. B. *J. Mater. Chem.* **2005**, *15*, 4783.
(36) Fuller, L. S.; Iddon, B.; Smith, K. A. *J. Chem. Soc., Perkin Trans. 1* **1997**, No. 22, 3465.
(37) Kline, R. J.; DeLongchamp, D. M.; Fischer, D. A.; Lin, E. K.; Richter, L. J.; Chabinyc, M. L.; Toney, M. F.; Heeney, M.; McCulloch, I. *Macromolecules* **2007**, *40*(22), 7960.

Scheme 1 [a]

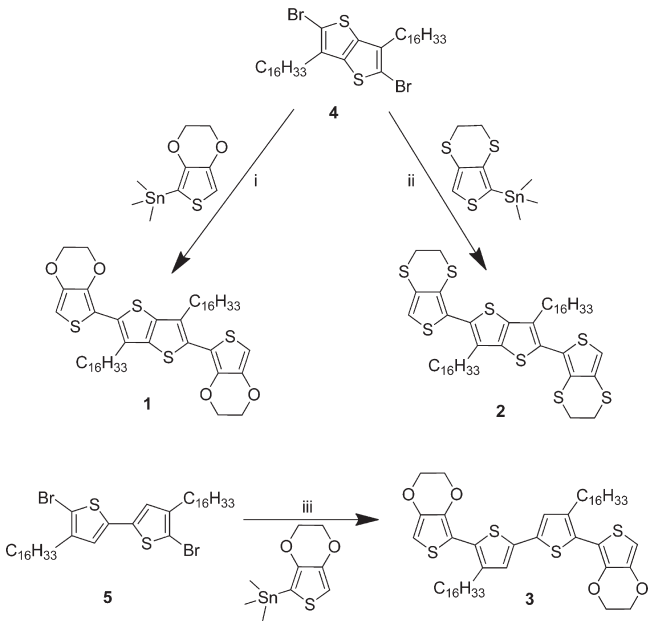

[a] Reagents and conditions: (i, ii, iii) $Pd(PPh_3)_4$, DMF, μW, 160 °C, 2 h.

conformation as a result of noncovalent S···O interactions between the thienothiophene core and the two EDOT units. The interatomic S···O distances were measured to be 2.87 Å, which is significantly shorter than the sum of the van der Waals radii for sulfur and oxygen (S + O = 3.32 Å).

Figure 2 shows the packing structure of compound **1**. The interplanar $\pi-\pi$ distances were measured to be 3.46 Å, which represent significant $\pi-\pi$ interactions. The alkyl side chains interdigitate and the molecule shows good close packing within the 2D sheet (Figure 2 left). The alkyl side chain interactions are known to be important in facilitating the growth of ordered crystalline microstructures.[38] The side-chain attachment density of a polymer is known to be related to the chemical structure of the monomer; it is therefore an intrinsic property of the polymer and is independent of processing history, M_W, or side-chain length.[37] Although the structure of **1** provides only some indication of how the conjugated chains may align in the polymer, the likelihood of the local geometry of the structure (EDOT-thienothiophene segments) persisting in the polymer is considered to be high. Electrochemistry and absorption studies support this assumption (vide infra).

Figure 3 shows the molecular structure of compound **2** in the crystalline state. In contrast to the planar structure of **1**, the molecular backbone of **2** is highly twisted. The dihedral angle between the thienothiophene core and the flanking EDTT units is close to being perfectly orthogonal (86.84°). The main cause of this is attributed to the unfavorable S···S interactions, which are known to twist the main chain in PEDTT.[35,39]

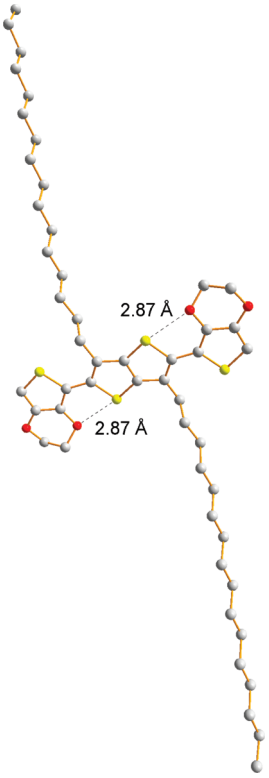

Figure 1. Molecular structure of compound **1**.

This twisted nature breaks conjugation within the molecule and thus raises the ionization potential. The alkyl chains in **2** are orientated almost at right angles to the thienothiophene core (88.75°). Figure 4 shows a packing diagram for compound **2**. No significant interdigitation or close-range interactions are apparent in the solid-state structure.

Electrochemistry and UV−Vis Spectroscopy. Cyclic voltammetry experiments were performed within DCM solutions of the monomers in 0.1 mmol concentration with a silver wire as pseudo reference electrode and 0.1 M concentration of tetrabutylammonium hexafluorophosphate ($TBAPF_6$) as the supporting electrolyte. A summary of the redox events for compounds **1**−**3** is shown in Table 1 and the cyclic voltammograms are represented in Figure 5. The EDOT-containing compound **1** exhibits an irreversible oxidation peak at +0.46 V and a second oxidation at +0.95 V. Compound **3** also shows irreversible oxidations at +0.37 V and +0.79 V. The presence of EDTT in **2** causes the oxidation to become quasi-reversible and shifted to a higher potential of +0.71/0.51 V. All three compounds have the same reduction peak apparent at −1.97 V. The absorption spectra for the three materials are depicted in Figure 6; they show that the maxima corresponding to the $\pi-\pi^*$ transitions vary significantly and are in the range 395−452 nm. Derivative **3** has a greater effective conjugation length and thus a lower HOMO− LUMO gap than **1**. The EDTT units in **2** have lowered the HOMO level relative to **1** by introducing a nonplanar conformation in the system, thus widening the HOMO−LUMO gap. The fused core of **1** and **2** has reduced the effective conjugation length of the molecules

(38) DeLongchamp, D. M.; Kline, R. J.; Lin, E. K.; Fischer, D. A.; Richter, L. J.; Lucas, L. A.; Heeney, M.; McCulloch, I.; Northrup, J. E. *Adv. Mater.* **2007**, *19*(6), 833.
(39) Pang, H.; Skabara, P. J.; Crouch, D. J.; Duffy, W.; Heeney, M.; McCulloch, I.; Coles, S. J.; Horton, P. N.; Hursthouse, M. B. *Macromolecules* **2007**, *40*(18), 6585.

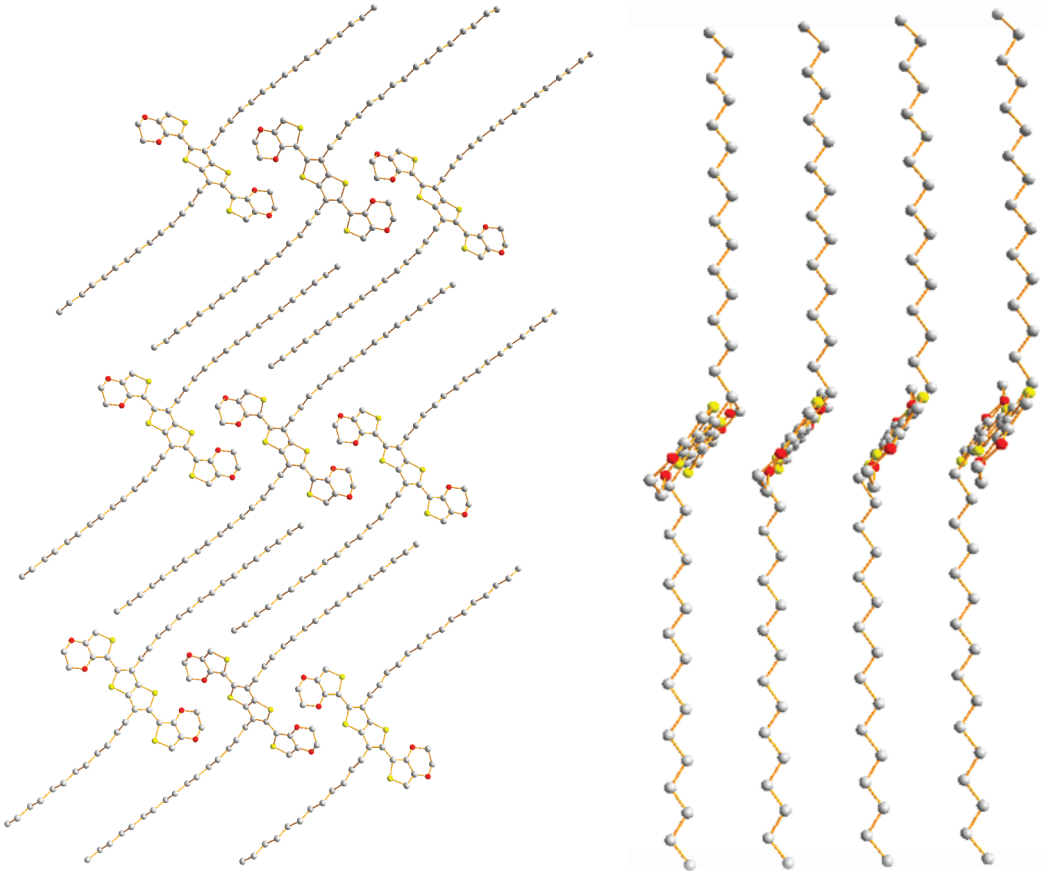

Figure 2. Packing diagrams of **1** viewed along the *b* axis (left) and showing alignment of the conjugated units (right).

and as such, lowered the HOMO levels slightly (0.24 eV). The thieno[3,2-*b*]thiophene unit has a higher aromatic stabilization energy than a single thiophene unit[40] and this serves to lower the HOMO level and thus widen the HOMO−LUMO gap. There is some discrepancy between the HOMO−LUMO gap calculated optically and that determined electrochemically (*ca.* 0.5−0.8 eV). The reason for this is that the EDOT and EDTT units contribute significantly to the electrochemically calculated HOMO−LUMO gap as they govern the ionization potential of the monomer. The same cannot be said for the optically calculated HOMO−LUMO gap, which is dependent on the effective conjugation length of the monomer.[41]

Polymers of compounds **1**, **2**, and **3** were grown onto a carbon electrode by repetitive oxidative cycling over the first oxidation wave. Table 2 shows a summary of the redox events associated with polymers **1**−**3**. The voltammogram (Figure 7) of poly(**1**) displays an oxidation peak at E_{1ox} = −0.33 V and a second, reversible oxidation is present at E_{2ox} = +0.31/+0.26 V. Poly(**2**) shows a quasi-reversible oxidation wave at E_{1ox} = +0.64/0.52 V and a second irreversible wave at E_{2ox} = +0.74 V. The band gap calculated for poly(**2**) is very similar to the HOMO−LUMO gap of **2** in its monomer form, indicative of the twisted nature of the polymer chain preventing extended conjugation through the system. The voltammogram of poly(**3**) shows an irreversible oxidation at E_{1ox} = −0.04 V and a second peak is apparent at E_{2ox} = +0.32/+0.25 V. All three polymer systems show a reduction wave present in the region of −2.0 to −2.1 V. It is unusual that the reduction onsets for the polymers are more negative than the monomer values, but the differences are small and within experimental error. Therefore, we assume that the LUMO remains largely unchanged on polymerization of compounds **1**−**3**.

In the case of poly(**1**) and poly(**3**), there is a large shift in the HOMO energies of the polymer compared to the monomers because of increased conjugation. Poly(**1**) has a band gap of 1.53 eV, the lowest of the three systems (see Table 2). This is because the polymer is held planar by noncovalent S···O interactions, causing the conjugation length of the molecule to be larger than either of the other systems. Poly(**3**) has a bithiophene central unit which can allow rotation around the 5,5′-linkage. This rotation can result in a deviation from planarity and subsequently[42] the ionization potential of poly(**3**) is higher than that of poly(**1**); the band gap is also greater. The band gap exhibited by poly(**2**) is wider than those of both of its analogues. This is due to nonplanarity in the polymer resulting from the EDTT units in the polymer chain,

(40) Skabara, P. J. Fused Oligothiophenes. In *Handbook of Thiophene-Based Materials*; Perepichka, I. F., Perepichka, D. F., Eds.; Wiley: New York, 2009; pp 219.
(41) Fieser, L. F.; Fieser, M.; Rajagopalan, S. *J. Org. Chem.* **1948**, *13*(6), 800.
(42) Ong, B. S.; Wu, Y.; Liu, P.; Gardner, S. *J. Am. Chem. Soc.* **2004**, *126*(11), 3378.

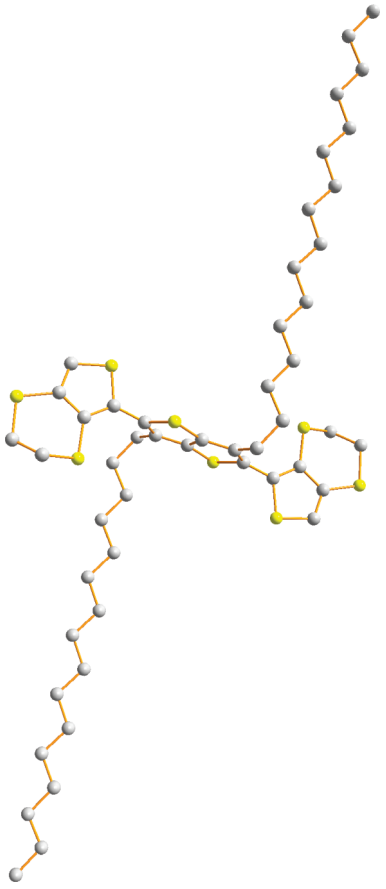

Figure 3. Molecular structure of compound **2**.

which are clearly seen to twist in the structure of compound **2.**

Spectroelectrochemistry. Polymers of **1** and **3** were grown onto indium tin oxide (ITO) coated glass by repetitive oxidative cycling. Growth of poly(**2**) was unsuccessful on this type of electrode because of poor adhesion of the polymer film on the substrate. Spectroelectrochemical measurements were recorded from 0.1 M solutions of $TBAPF_6$ in acetonitrile. Both polymer films were dedoped by repetitive cycling over a range in which the polymer shows no electroactivity (i.e., between the first oxidation and reduction waves). The optical band gaps for poly(**1**) and poly(**3**), calculated from the onset of the longest wavelength absorption peaks, were found to be 1.74 and 1.84 eV, respectively. The UV−vis spectra of the polymer-coated slides were measured as the potential applied to the samples was increased in 100 mV increments over the range −700 to +2000 mV (see Figures 8 and 9). Poly(**1**) shows a decrease in the $\pi-\pi^*$ absorption band caused by disruption to the conjugated chain through oxidation, and a new band emerges between 600 and 1000 nm. The latter is most intense at +500 mV and is attributed to the formation of polarons in the polymer chain. The polaron absorption tails off at ca. +800 mV and a second band appears in the same region after 1500 mV suggesting the formation of bipolarons along the polymer chain. In contrast to the spectroelectrochemistry of PEDOT,[34] the polaron band for poly(**1**) is blue-shifted and the second transition for the latter is absent in PEDOT. In poly(**3**), the $\pi-\pi^*$ absorption band decreases in a similar fashion to poly(**1**). A new band due to polaron formation appears in the region 600−1000 nm and it reaches a maximum by +300 mV. This polaron band begins to diminish after +600 mV and no further transitions are apparent. The polymer film appears to detach from the ITO electrode as higher potentials are approached. The optical transparency of the polymers in their doped states (i.e., the almost complete disappearance of the $\pi-\pi^*$ bands) marks these materials as promising candidates for electrochromic devices.[10]

Time of Flight Measurements. Because the monomers studied in this work exhibited interesting packing in the crystalline state, we investigated the charge transport properties of films of compounds **1** and **2** by the charge generation layer time-of-flight (CGL-TOF) method. For these measurements, solutions of monomers were made to concentrations of 40 mg mL^{-1} in chlorobenzene. Films were spin-coated onto an ITO substrate at speeds of 800−1000 rpm to obtain films around 100−200 nm thick. The samples were then transferred to an evaporator where, under high vacuum, a 10 nm layer of the perylene dye (Lumogen Red) followed by 100 nm of aluminum was deposited through a shadow mask to define the active area of approximately 6 mm^2. Testing was undertaken by exciting the charge generation layer through the ITO and monomer layer. Charge carriers were generated within the perylene layer by excitation from a 500 ps pulse of a dye laser at a wavelength of 580 nm, which is the peak of the absorption spectrum of Lumogen Red. At this excitation wavelength the monomers are completely transparent (see Figure 6). The highest occupied molecular orbital of the Lumogen Red was estimated from cyclic voltammetry measurements to be 6.2 eV from the vacuum level, enabling hole injection into the monomer layer. The packet of charge carriers was then swept through the device under an applied field, and the transit time (t_{tr}) measured using a digital storage oscilloscope. The aluminum electrode was biased positively and the photocurrent signal detected from the ITO (see Figure 10). The applied bias led to the electrons photogenerated in the perylene dye layer being removed from the device at the aluminum electrode and holes being injected into the monomer from the perylene dye and consequently swept across the device to be collected at the ITO electrode. Thus the measured photocurrent transients are hole currents. Hole mobilities, μ, were deduced from the transit times, t_{tr}, via the relation $\mu = d^2/Vt_{tr}$, where d is the film thickness and V the applied voltage. The sample was mounted in a vacuum cryostat at room temperature. The RC time constant of the measurement circuit was always selected to be $\leq 20\ t_{tr}$. The total charge injected into the film was kept around 2−3% CV in all cases, where C is the capacitance of the device and V the applied voltage.

Figure 11 shows the hole photocurrent transient on linear and log−log scales for a film of compound **1** at room temperature for an applied electric field $E = 5.1 \times 10^5$ V cm^{-1}. The absence of a clear plateau

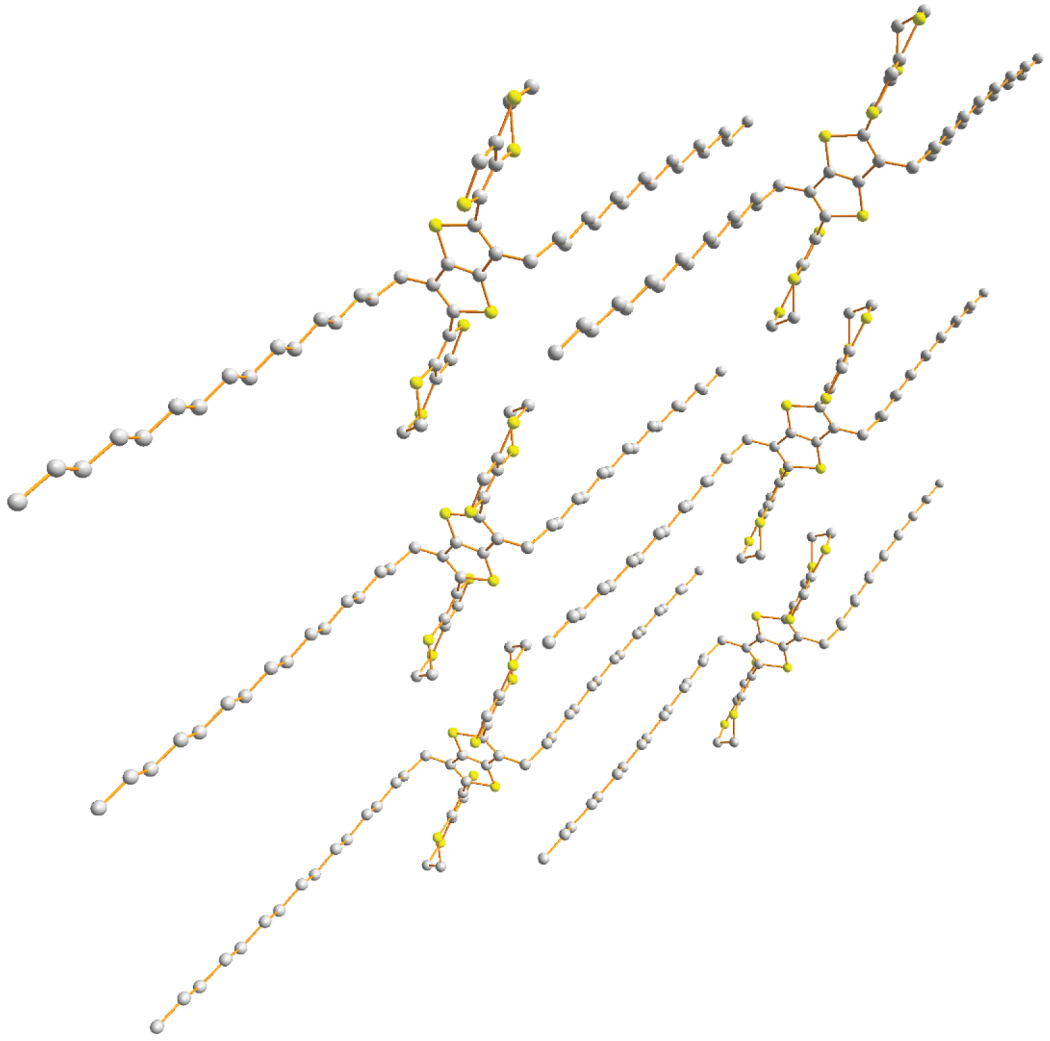

Figure 4. Packing diagram of **2**.

Table 1. Optical and Electrochemical Properties of Monomers 1−3

	E_{1ox} (V)	E_{2ox} (V)	E_{1red} (V)	HOMO (eV)[a]	LUMO (eV)[a]	electrochemical E_g (eV)	λ_{max} (nm)	optical E_g (eV)[b]
1	+0.46	+0.95	−1.98	−5.18	−2.97	2.21	411	3.01
2	+0.71/0.51	+1.00	−1.97	−5.42	−2.97	2.45	395	3.14
3	+0.37	+0.79	−1.97	−5.08	−2.96	2.12	452	2.74

[a] The HOMO and LUMO values shown were calculated from the peak onset of the respective redox wave. All values have been referenced to the HOMO of ferrocene which is known to be −4.8 eV. [b] The optical HOMO−LUMO gap for each compound was calculated from the onset of the longest wavelength peak.

in the photocurrent transient on a linear scale is indicative of highly dispersive charge transport behavior. In order to estimate the transit time (t_{tr}) a log−log plot was necessary, which allowed measurement of the transit time from the change of slope of the photocurrent transient, t_{tr} = 0.95 μs. The transit time corresponds to a mobility of 3.5×10^{-5} cm^2 V^{-1} s^{-1}.

Figure 12 shows the hole photocurrent transient on linear and log−log scales for a film of compound **2** at room temperature for an applied electric field $E = 5.1 \times 10^5$ V cm^{-1}. Again the absence of a clear plateau in the photocurrent transient in linear scale is indicative of highly dispersive charge transport behavior. In order to estimate the transit time (t_{tr}) a log−log plot was necessary, which allowed measurement of the transit time from the change of slope of the photocurrent transient, t_{tr} = 2.3 μs. The transit time corresponds to a mobility of 1.4×10^{-6} cm^2 V^{-1} s^{-1}.

Our measurements give the hole mobility in the direction perpendicular to the substrate, and we have studied its field dependence, as shown in Figure 13. As the electric field is increased from 2×10^5 to 8×10^5 V cm^{-1}, the hole mobility increases from 2×10^{-5} to 4×10^{-5} cm^2 V^{-1} s^{-1} for **1** and from 6.3×10^{-6} to 1.5×10^{-5} cm^2 V^{-1} s^{-1} for compound **2**. The difference in conformation between compounds **1** and **2** in solution state is indicated by the corresponding values for λ_{max} in Figure 6. Figure 14 shows the absorption spectra for **1** and **2** in the thin-film state, using the same conditions for processing as those used for the CGL-TOF experiments. The difference in

absorption maxima is even greater in the solid state, with the onset of the longest wavelength absorption in **2** being ca. 90 nm hypsochromically shifted compared to that of compound **1**. In general, it should be expected that twisting the arrangement of aryl rings in a conjugated chain will lead to a lowering in mobility because of a decrease in π-orbital overlap. The increased mobility seen in compound **1** compared to monomer **2** is commensurate with the nonplanar conformation of the latter in the thin-film state.

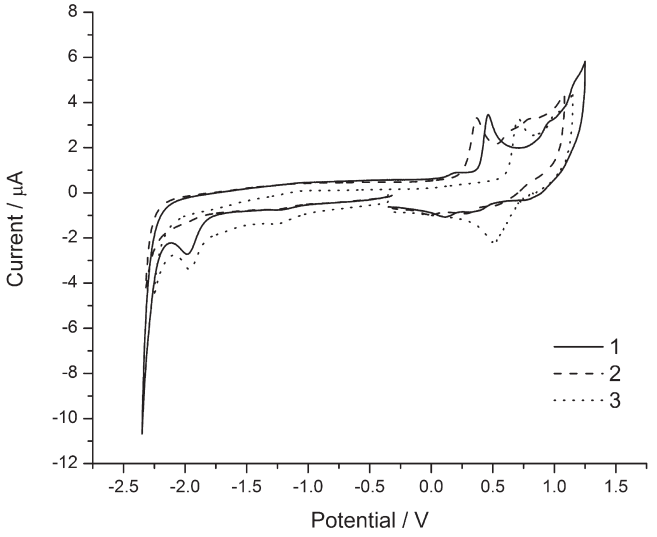

Figure 5. Cyclic voltammograms of compounds **1**−**3** in DCM solution (carbon working electrode, silver wire pseudoreference, $TBAPF_6$ as the supporting electrolyte (0.1 M), substrate concentration 1×10^{-4} M, scan rate 100 mV/s). The data are referenced to the Fc/Fc^+ redox couple.

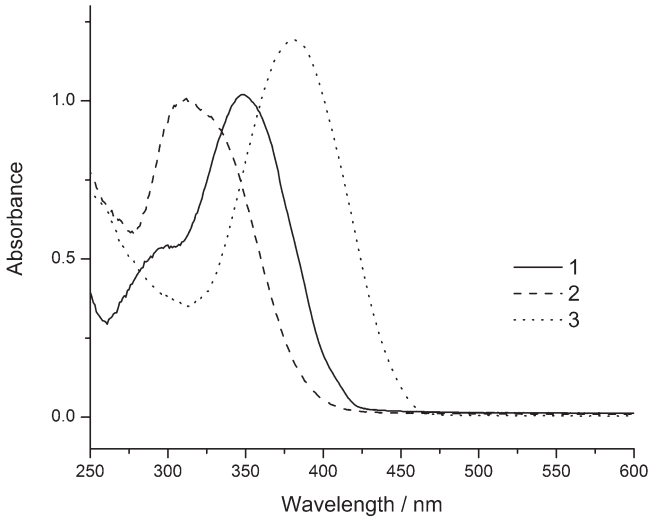

Figure 6. UV−vis absorption spectra of compounds **1**−**3** in dichloromethane solution.

Summary. Three new monomers have been synthesized and their corresponding polymers have been grown electrochemically. Where possible, they have been characterized by absorption spectroscopy, cyclic voltammetry and UV−vis spectroelectrochemistry. The X-ray crystal structure of compound **1** shows strong noncovalent

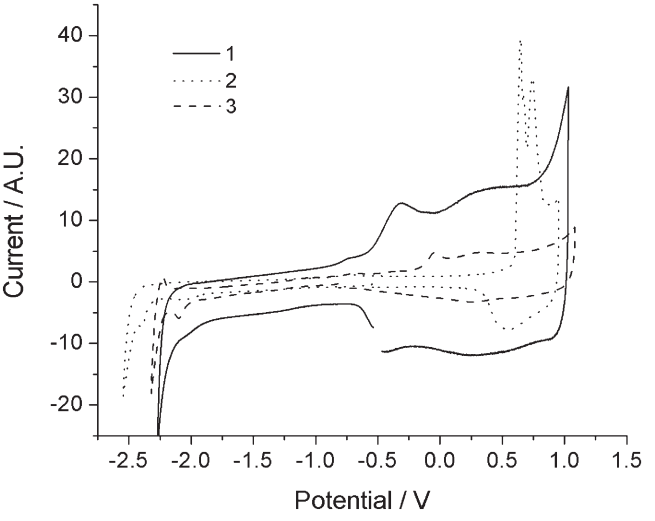

Figure 7. Cyclic voltammograms of poly(**1**), poly(**2**), and poly(**3**) as thin films deposited on a glassy carbon working electrode using a silver wire pseudoreference electrode, Pt wire counter electrode, and $TBAPF_6$ as the supporting electrolyte (0.1 M) in dichloromethane at a scan rate of 100 mV s^{-1}. The data are all referenced to the Fc/Fc^+ redox couple.

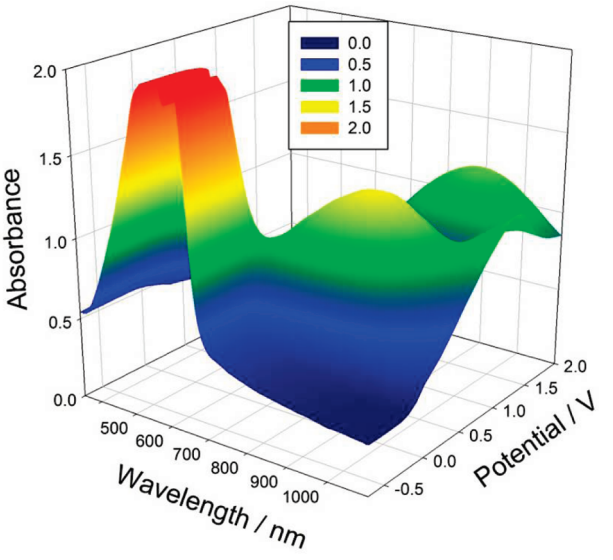

Figure 8. Spectroelectrochemical plot of poly(**1**) film coated on ITO working electrode, with platinum gauze counter electrode and silver wire reference. The film was measured over the potential range −0.7 V to +2.0 V in a DCM solution containing 0.1 M $TBAPF_6$ as supporting electrolyte.

Table 2. Electrochemical Properties of Polymers 1−3

	E_{1ox}(V)	E_{2ox}(V)	E_{1red} (V)	HOMO (eV)	LUMO (eV)	$E_g{}^a$ (eV)
poly(**1**)	−0.33	+0.31/+0.26	−2.02	−4.24	−2.71	1.53
poly(**2**)	+0.64/0.52	+0.74	−2.05	−5.39	−2.9	2.49
poly(**3**)	−0.04	+0.32/+0.25	−2.1	−4.66	−2.72	1.94

[a] The HOMO and LUMO values shown were calculated from the peak onset of the respective oxidation/reduction waves. All values have been referenced to the HOMO of ferrocene, which is known to be −4.8 eV.

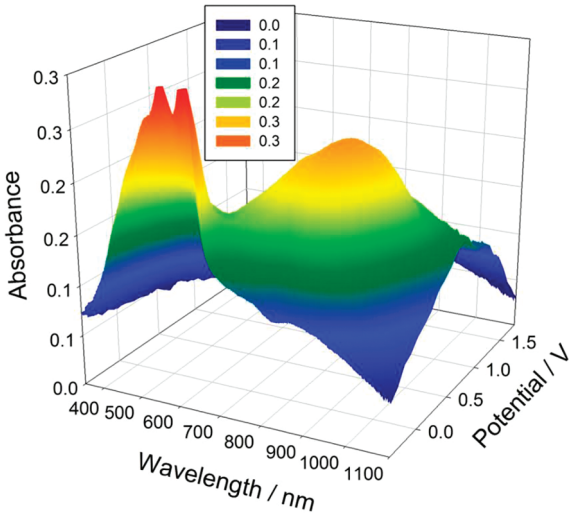

Figure 9. Spectroelectrochemical plot of poly(**3**) film coated on ITO working electrode, with platinum gauze counter electrode and silver wire reference. The film was measured over the potential range −0.4 V to +1.8 V in a DCM solution containing 0.1 M $TBAPF_6$ as supporting electrolyte.

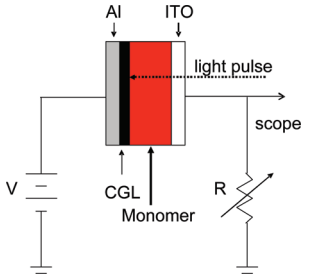

Figure 10. CGL-TOF schematic setup for measurements on compounds **1** and **2**.

S···O interactions and side-chain interdigitation, along with close $\pi-\pi$ stacking between molecular planes. Poly(**1**) has the lowest band gap of the three polymers measured and this is attributed to a rigid, planar structure. Compound **2** is severely twisted between the EDTT and thienothiophene units because of unfavorable S···S interactions, which affects the properties of the system by widening the HOMO−LUMO gap and lowering the HOMO energy level. Poly(**2**) has a band gap almost the same as the HOMO−LUMO gap measured in its monomer form, indicating that the local conformation around the thienothiophene-EDTT segment remains the same as in the monomer and that the EDTT−EDTT repeat units in the polymer are also significantly twisted, leading to very short effective conjugation no greater than the monomer (**2**). Compound **3** has the smallest HOMO−LUMO gap of the monomers because it has the greatest effective conjugation length. However, the corresponding polymer can rotate around the 5,5′-bithiophene linkage, thereby limiting the conjugation length, and therefore its band gap is not as low as may be expected. CGL-TOF measurements show that compound **1** has a higher mobility than **2**, which is expected for a more planar molecule with superior π-orbital overlap in the bulk solid.

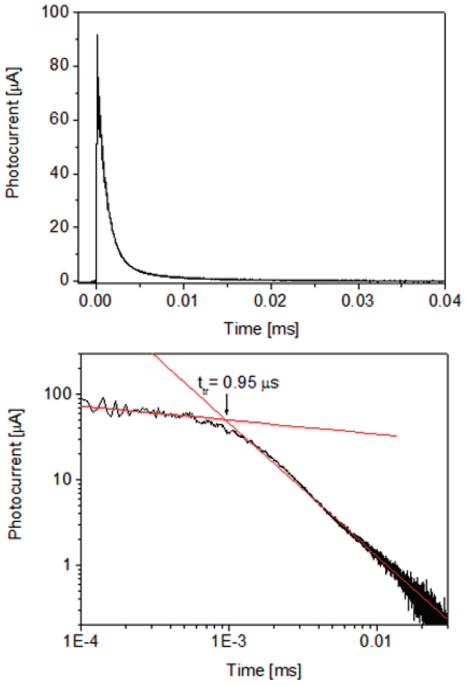

Figure 11. Hole photocurrent transient on linear (top) and log−log scale (bottom) for a film of compound **1**, at room temperature for an applied electric field $E = 5.1 \times 10^5$ V cm^{-1}.

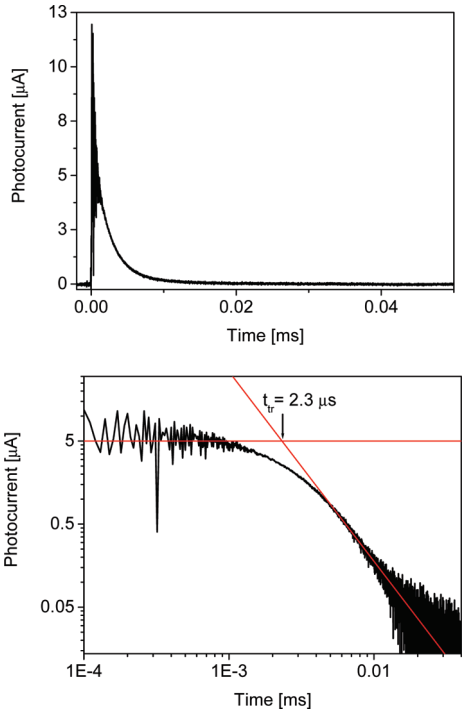

Figure 12. Hole photocurrent transient on linear (top) and log−log scale (bottom) for a film of compound **2** at room temperature for an applied electric field $E = 5.1 \times 10^5$ V cm^{-1}.

Experimental Section

General. ^{1}H and ^{13}C NMR spectra were recorded from deuterated chloroform ($CDCl_3$) on a Bruker DRX instrument at 500 MHz unless otherwise stated; chemical shifts are given in ppm and *J* values in Hz. Melting points were measured using a Stuart Scientific SMP1Melting Point apparatus and are uncorrected. Absorption spectra were measured on a Unicam UV 300 spectrophotometer. Cyclic voltammetry and spectroelectrochemical measurements were performed using a CH

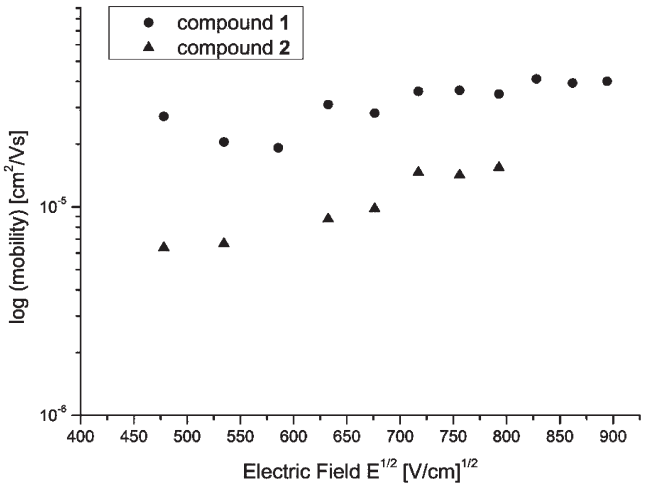

Figure 13. Room-temperature mobility vs electric field for the two films investigated.

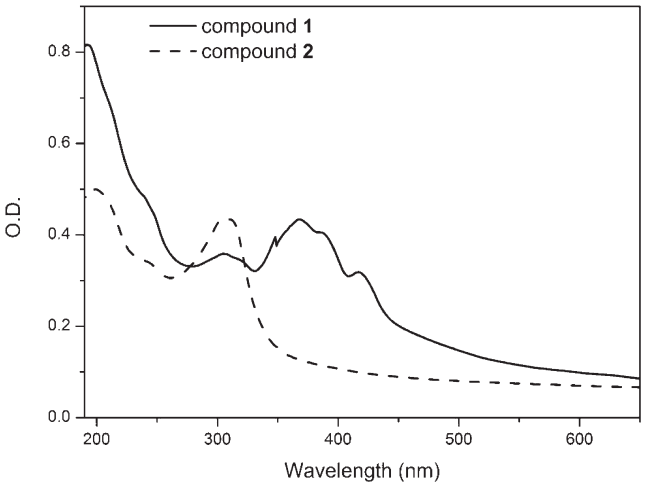

Figure 14. Absorption spectra of thin films of compounds **1** and **2**.

Instruments 660A Electrochemical Workstation with *iR* compensation. Solvents used for electrochemical experiments were DCM and MeCN and were degassed prior to measurement using argon. Where relevant, the solvent contained the analyte molecule in concentrations of ca. 1×10^{-3} M, together with $TBAPF_6$ (0.1 M) as the supporting electrolyte. For all reactions, the organic extracts were combined and dried over $MgSO_4$ and the solvents were removed using a rotary evaporator (vacuum supplied by low vacuum pump); where necessary, a high vacuum pump was used to remove residual solvent. 3-Bromothiophene was supplied by Aldrich and 5,5′-dibromo-4,4′-dihexadecyl-2,2′-bithiophene was supplied by Merck chemicals.

5,5′-(3,6-Dihexadecylthieno[3,2-b]thiophene-2,5-diyl)bis(2,3-dihydrothieno[3,4-b][1,4]dioxine) 1. 2,5-Dibromo-3,6-dihexadecylthieno[3,2-b]thiophene **12** (300 mg, 0.4 mmol), (2,3-dihydrothieno[3,4-b][1,4]dioxin-5-yl)trimethylstannane (270 mg, 8.85 mmol), and $Pd(PPh_3)_4$ (50 mg, 0.1 equiv.) were added to a dry microwave vial (2−5 mL type) and the vial was purged with dry nitrogen, after which DMF (3 mL) was added. The reaction mixture was heated in the microwave at 160 °C for 2 h. The reaction mixture was then poured into chloroform (100 mL) and washed with 2 M HCl solution (2 × 100 mL) and water (2 × 100 mL). The organic extracts were combined and dried over $MgSO_4$. The crude product was purified by column chromatography on silica. DCM/hexane (1:2) eluted **1** as a yellow solid (0.25 g, 72%). mp 113 °C. δ_H 0.89 (6H, t, *J* 7.0, 2 × CH_3), 1.26 (52H, m, 26 × CH_2), 1.73 (4H, m, 2 × CH_2), 2.79 (4H t, *J* 7.7, 2 × $ArCH_2$), 4.27 (8H, m, 4 × CH_2), 6.40 (2H, s, 5-H). δ_C (500 MHz, $CDCl_3$) 14.1, 22.7, 28.9, 29.3, 29.6, 31.9, 64.5, 64.8, 99.4, 110.8, 127.8, 133.4, 138.5, 139.1, 141.5. Anal. Calcd for $C_{50}H_{76}S_4O_4$ C, 69.07; H, 8.81; S, 14.75% found; C, 69.08; H, 8.85; S, 14.85%. MS: *m*/*z*, MALDI, M^+ 868 (100%).

5,5′-(3,6-Dihexadecylthieno[3,2-b]thiophene-2,5-diyl)bis(2,3-dihydrothieno[3,4-b][1,4]dithiine) 2. 2,5-Dibromo-3,6-dihexadecylthieno[3,2-b]thiophene **12** (300 mg, 0.4 mmol), (2,3-dihydrothieno[3,4-b][1,4]dithiin-5-yl)trimethylstannane (300 mg, 0.89 mmol) and $Pd(PPh_3)_4$ (50 mg, 0.1 equiv.) were added to a dry microwave vial (2−5 mL type) and the vial was purged with dry nitrogen, after which DMF (3 mL) was added. The reaction mixture was heated in the microwave at 160 °C for 2 h. The reaction mixture was then poured into chloroform (100 mL) and washed with 2 M HCl solution (2 × 100 mL) and water (2 × 100 mL). The organic extracts were combined and dried over $MgSO_4$. The crude product was purified by column chromatography on silica. DCM/hexane (1:3) eluted **2** as a waxy pale yellow solid (0.228 g, 61%). mp 73−74 °C. δ_H 0.88 (6H, t, *J* 6.9, 2 × CH_3), 1.25 (52H, m, 26 × CH_2), 1.70 (4H, m, 2 × CH_2), 2.67 (4H, t, *J* 7.9, 2 × CH_2), 3.23 (8H, s, 4 × CH_2), 7.06 (2H, s, 5-H). δ_C 14.12, 22.70, 27.41, 27.98, 28.70, 29.30, 29.37, 29.54, 29.71, 31.93, 119.14, 125.47, 126.12, 126.97, 127.89, 135.70, 139.53. MS: *m*/*z*, MALDI, M^+ 932.54 (100%).

5,5′-(4,4′-Dihexadecyl-2,2′-bithiophene-5,5′-diyl)bis(2,3-dihydrothieno[3,4-b][1,4]dioxine) 3. 5,5′-Dibromo-4,4′-dihexadecyl-2,2′-bithiophene (300 mg, 3.88 mmol), (2,3-dihydrothieno[3,4-b][1,4]dioxin-5-yl)trimethylstannane (260 mg, 8.54 mmol) and $Pd(PPh_3)_4$ (50 mg, 0.1 equiv.) were added to a dry microwave vial (2−5 mL type) and the vial was purged with dry nitrogen after which DMF (3 mL) was added. The reaction mixture was heated in the microwave at 160 °C for 2 h. The reaction mixture was then poured into chloroform (100 mL) and washed with 2 M HCl solution (2 × 100 mL) and water (2 × 100 mL). The organic extracts were combined and dried over $MgSO_4$. The crude product was purified by column chromatography on silica. DCM/hexane (1:3) eluted **3** as a yellow solid (219 mg, 63%). mp 93−94 °C. δ_H 0.88 (6H, t, *J* 6.9, 2 × CH_3), 1.26 (52H, m, 26 × CH_2), 1.63 (4H, m, 2 × CH_2), 2.67 (4H, t, *J* 7.9, 2 × CH_2), 4.28 (8H, m, 4 × CH_2), 6.37 (2H, s, 5-H), 6.98 (2H, s, Ar CH). δ_C 14.12, 22.70, 29.37, 29.49, 29.58, 29.62, 29.70, 64.51, 64.88, 98.84, 110.46, 125.56, 126.19, 136.09, 138.12, 141.43, 141.49. MALDI, M^+ 894.60 (100%).

X-ray Crystallography. Single crystals of compounds **1** and **2** were obtained from the slow evaporation of DCM-hexane solutions. Those of **2** were examined on a Bruker-Nonius APEX2 diffractometer with rotating-anode Mo-*K*α radiation (λ = 0.71073 Å), using standard procedures and software. Those of **1** were of rather poorer quality, very thin, and weakly diffracting, requiring the use of synchrotron radiation (λ = 0.6941 Å), and giving a lower-precision result; the basic features of the structure are, however, unambiguous. Full crystallographic details are available in the Supporting Information.

Acknowledgment. F.V. and P.J.S. thank the EPSRC for funding (EP/E027431). The EPSRC is also thanked for funding the National Crystallography Service at Southampton and Newcastle/Daresbury, and STFC is thanked for access to synchrotron facilities.

Supporting Information Available: Crystallographic data files for structures **1** and **2** (CIF). This material is available free of charge via the Internet at http://pubs.acs.org.